© 2012 THOSS Media & DE GRUYTER DOI 10.1515/aot-2012-0032 — Adv. Opt. Techn. 2012; 1(4): 323–334

**Research Article**

Tomoyuki Matsuyama[a,]*, Yasushi Mizuno and Daniel G. Smith

# Imaging optics on scanner for SMO generation process

**Abstract:** The k1 factor continues to be driven downward, in order to enable the 22-nm feature generation and beyond. Such a low k1 factor tends to lead to extremely small process windows. For such demanding imaging challenges, it is not only necessary for each unit, contributing to the imaging system, to be driven to its ultimate performance capability, but also that active techniques that can expand the process window and the robustness of the imaging against various kinds of imaging parameters be implemented. One such technique is source and mask optimization (SMO). In this paper, we study the effect of SMO. Furthermore, we discuss how to realize the SMO solution in the imaging system setup on the scanner. The setup process includes freeform pupilgram generation (source intensity distribution on the pupil) and pupilgram adjustment.

**Keywords:** illumination system; pupilgram; source and mask optimization.

[a] Present address: Nikon, Precision Equipment Company, 201-9 Miizugahara, Kumagaya 360-8559, Japan
***Corresponding author: Tomoyuki Matsuyama,** Nikon Corporation, 210-9 Mizugahara, Kumagaya, Saitama 360-8559, Japan, e-mail: Matsuyama.Tomoyuki@nikonoa.net
**Yasushi Mizuno:** Nikon Corporation, 210-9 Mizugahara, Kumagaya, Saitama 360-8559, Japan
**Daniel G. Smith:** Nikon Research Corp. of America, 12490 N Rancho Vistoso Blvd., Tucson, AZ 85737, USA

## 1 Introduction

Finer and finer device patterning has been required for semiconductor manufacturing as the number of transistors in a chip has increased rapidly. In order to meet this requirement, we have continued to increase the numerical aperture (NA), shortened the exposure light wavelength, and reduced the k1 factor, which is defined in Eq. (1).

$$R=k1\frac{\lambda}{NA} \quad (1)$$



where R is the resolution limit, which is usually defined as the half pitch of the minimum resolution spatial period, λ is the wavelength, and NA is the numerical aperture of the projection lens.

Today, a 22-nm feature size patterning is needed for device manufacturing. Although extreme ultraviolet lithography (EUVL) technology with a 13.5-nm wavelength exposure light is being developed, there are still some items, which must be finalized, to apply this technology to practical semiconductor manufacturing in the required time frame. Therefore, we need to use the current generation exposure tools, which use the 193-nm wavelength ArF excimer laser for illumination. However, the 22-nm feature sizes then require a significantly lower k1 factor and an extremely small process window, which is usually defined as a combination of the exposure latitude and the focus margin for generating acceptable imaging performance. Owing to the extremely small process window available for such demanding imaging challenges, it is necessary that active techniques be implemented to expand the process window and robustness of the imaging against various kinds of imaging parameters. Source and mask optimization (SMO) is a promising candidate technique.

An intelligent illuminator [1] is proposed to realize the pupilgram solutions produced by the SMO. The many degrees of adjustment freedom allowed by an intelligent illuminator can be used not only for the purposes of realizing the pupilgram solution but also to enable high-accuracy optical proximity effect (OPE) matching.

## 2 Source and mask optimization

The objective of the SMO is to maximize the number of critical patterns that have sufficient imaging performance, such as focus margin, dose latitude, etc., with the same lens NA and wavelength. In this section, we introduce the concept of the SMO by showing our R&D-based SMO tool and some numerical experiment results using the SMO tool.

 © 2012 THOSS Media & DE GRUYTER

## 2.1 Source and mask optimization tool

We have developed the R&D-based SMO software for the effectiveness of the SMO in improving process margin or reducing the k1 factor, for the coming generation of feature sizes.

This prototype SMO tool has two modes. One is the freeform mode, and the other is the constrained mode. The freedom of illumination parameters are the same between the two modes. However, in the freeform mode, the SMO tool has a greater freedom in the *mask* parameters, including the ability to incorporate continuous amplitude transmission distributions and phase distributions. On the other hand, the constrained optimization mode allows only a limited freedom in the mask parameters. Figure 1 indicates the concept of input, output, and calculation flow of the software.

As input, we have:

1. Critical target pattern: Target image intensity distribution for critical pattern, which has a small process margin compared with other patterns.
2. Starting mask: This is optional. This algorithm can generate the starting mask data, defined by the amplitude transmission distribution and phase distribution, from the target image assuming the initial source shape for freeform mode. The target pattern itself can be the starting mask for the constrained mode.
3. Starting source: The user can input any illumination source shape, which can be defined as a conventional resolution enhancement technology (RET) illumination, such as annular illumination, dipole illumination, quadruple illumination, etc.
4. Merit function and constrains:
   – Merit function: Image contrast and log slope at the edge of the pattern is the merit function for the freeform mode. For the constrained mode, a common process window and optical proximity effect (OPE) error are the targets for the optimization. OPE error is usually defined as the pattern size difference between a given dimension in an exposed pattern and the target over a range of pattern spatial frequencies.
   – Constraints: For an illumination distribution, the minimum illumination area can be defined. This is to prevent unreasonable illumination solutions, which cannot be realized on the actual tool.

During optimization, the mask optimization and source optimization are performed sequentially, and some number of iterations is needed to converge on a solution.

The outputs of the SMO are:

1. Mask design: Amplitude transmission distributions and phase distributions in the freeform mode, and mask bias and subresolution assist feature (SRAF) settings in the constrained mode.
2. Source design: Intensity distribution of the source.
3. Performance report: Intensity distribution of obtained images with various defocus values for the freeform mode and process window and OPE through focus for the constrained mode.

## 2.2 Numerical experiment of SMO capability

We have performed optimization tests to understand the capability of the SMO tool in use. The two modes of the SMO tool, the freeform optimization mode, and the constrained optimization mode were evaluated separately. In the case of the constrained mode, we have compared the

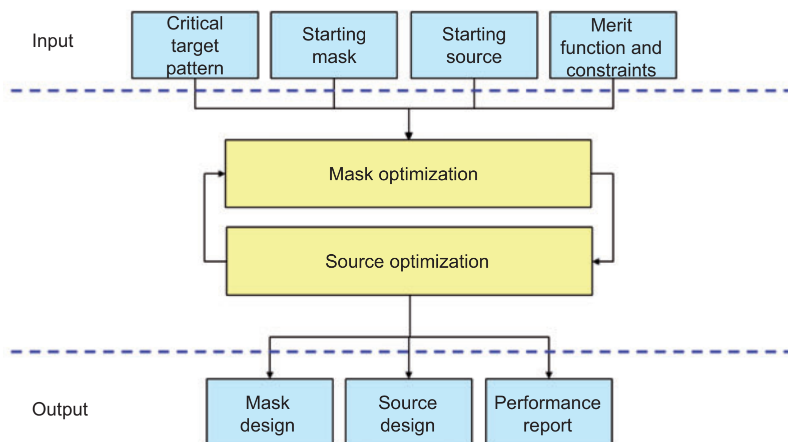


**Figure 1** Conceptual flow chart of the prototype SMO.

imaging performance with the conventional RET illumination result.

### 2.2.1 Freeform optimization

The condition of optimization is shown below:

1. Target image:
   – In the illustration in Figure 2, the black circle point should be dark, white circle points should be bright, and the red circle points are used for calculating the image slope at the edge of the image.
2. Target of the optimization:
   – Image contrast.
   – Image log slope at red point.
3. Parameters:
   – Mask amplitude transmission distribution.
   – Mask phase distribution.
   – Illumination intensity distribution (pupilgram).
4. Imaging parameters:
   – NA: 1.35.
   – Maximum sigma: 0.98.
   – Wavelength: 193 nm.
   – Polarization status: unpolarized light.
   – Optical image in water (n=1.44).

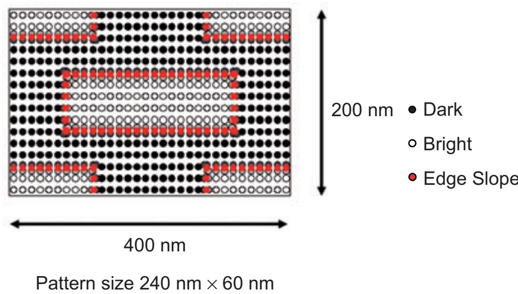


**Figure 2** Target image for freeform optimization.

The results of the freeform optimization are shown in Figure 3. As the number of optimization cycles increases (illumination optimization cycles are shown), the intensity distribution approaches the target image even for the defocused images. The illumination source intensity distribution, mask amplitude transmission distribution, and phase distribution also change drastically during optimization. However, as seen in the mask amplitude transmission distribution and phase distribution, this mask may be far beyond the current mask-fabrication capability. Therefore, the optimization with the more constrained mask patterns should be studied, and the constrained mode was developed for this reason.

### 2.2.2 Constrained optimization

Conditions for the constrained optimization are show bellow:

1. Imaging targets:
   – 45 nm vertical line pattern.

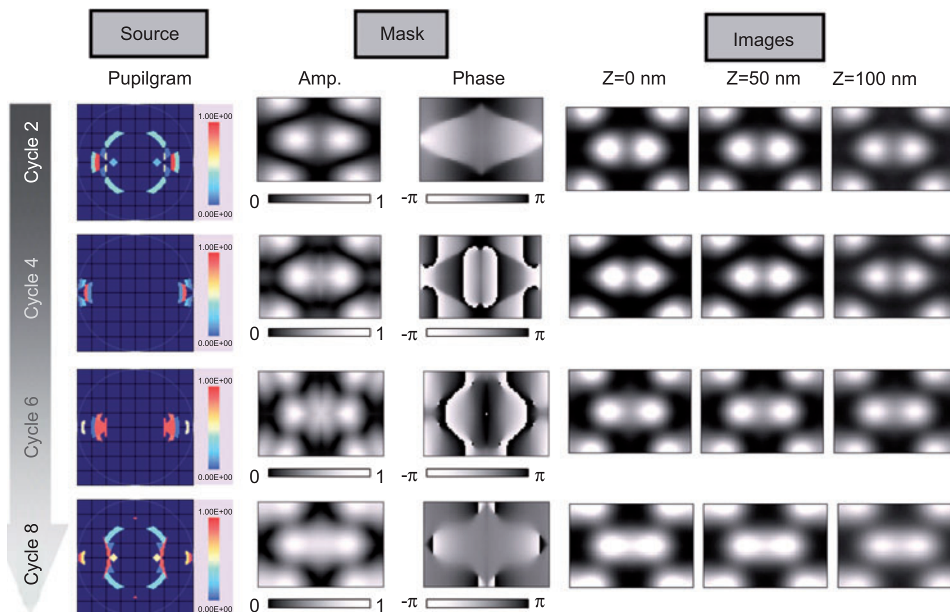


**Figure 3** Results of freeform optimization.

 © 2012 THOSS Media & DE GRUYTER

   – Pitch: 110 nm, 120 nm, 140 nm, 160 nm, 180 nm, 200 nm, 300 nm, 500 nm.
2. Optimization target:
   – To maximize the common process window area.
   – To minimize thru focus on the OPE.
3. Optimization parameters (shown in Figure 4):
   – Mask bias.
   – SRAF width and position.
   – Illumination pupilgram.
4. Imaging condition:
   – NA: 1.30.
   – Wavelength: 193 nm.
   – Polarization status: Y-polarized light.
   – Optical image in water (n=1.44), ±10% CD.

Before looking at the SMO results, an optimization solution with a conventional RET using the bowtie-type illumination is shown in Figure 5 as a reference. The mask setting for this is also shown in Table 1. The SMO illumination solution and the mask settings are shown in Figure 6 and Table 2.

As we can see from this example, a very complicated pupilgram is obtained by the SMO. The imaging performance comparison between the conventional RET and the SMO is shown in Figure 7. Obvious improvement of the OPE error and the common process window area are seen for the SMO results.

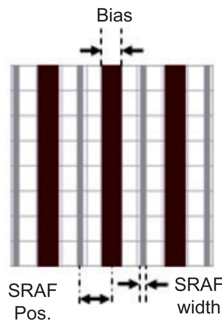


**Figure 4** Optimization mask parameters.

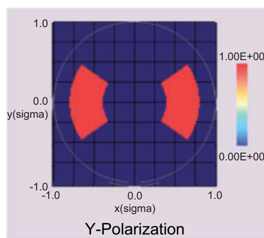


**Figure 5** Conventional RET with bowtie dipole illumination and mask settings.

| Pattern pitch (nm) | 110 | 120 | 140 | 160 | 180 | 200 | 300 | 500 |
|---|---|---|---|---|---|---|---|---|
| Line width (nm) | 45.0 | 41.1 | 40.0 | 41.3 | 48.0 | 53.6 | 53.8 | 44.0 |
| SRAF-center (nm) | 0 | 0 | 0 | 0 | 0 | 95 | 100 | 100 |
| SRAF-width (nm) | 0 | 0 | 0 | 0 | 0 | 10 | 18 | 18 |

**Table 1** Mask settings for conventional RET with bowtie dipole illumination.

# 3 Freeform pupilgram generation

The results of the source mask optimizations usually produce a pupilgram that is more complicated than the conventional parametric pupilgrams. So, we must have some way of determining how to generate the pupilgrams on the scanner that are as close as possible to the solution pupilgrams. We can generate the freeform pupilgram by both sPURE and the intelligent illuminator unit [2]. sPURE is an optical element that generates any shape, any fixed-shape far-field pupilgram.

## 3.1 Degree of pupilgram freedom (DPF)

To start the discussion of the requirements for freeform illumination, we define a parameter we call the 'degree of pupilgram freedom', as detailed below. The conceptual diagram of degree of the pupilgram freedom is shown in Figure 8.

Degree of pupilgram freedom=(grayscale level)×(total number of grids in the pupil).

## 3.2 Grayscale control

Figure 9A shows a comparison of the generated pupilgrams. In this example, the target pupilgram shape is defined to be an inverse cone shape. The effect of a large number of DPF is observed in the comparison. The OPE difference from the target pupilgram for the different numbers

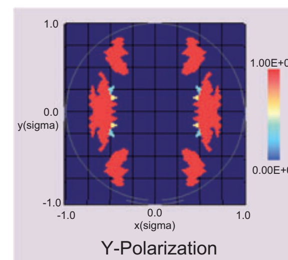


**Figure 6** SMO solution illumination.

| Pattern pitch (nm) | 110 | 120 | 140 | 160 | 180 | 200 | 300 | 500 |
|---|---|---|---|---|---|---|---|---|
| Line width (nm) | 59.6 | 64.9 | 65.9 | 64.3 | 67.6 | 76.4 | 82.1 | 79.1 |
| SRAF-Center (nm) | 0 | 0 | 0 | 0 | 0 | 0 | 117.7 | 115.5 |
| SRAF-width (nm) | 0 | 0 | 0 | 0 | 0 | 0 | 18.3 | 37.0 |

**Table 2** Mask settings for SMO result.

of DPF is shown in Figure 9B. If we allow an OPE difference of 0.5 nm, more than $10^4$ DPF is required. If we use a larger value of DPF, a better OPE performance is obtained.

We have also evaluated the accuracy of the intensity modulation with different numbers of DPF. For this evaluation, we use an example solution of the source mask optimization with the typical 1D NAND flash memory pattern shown in Figure 10G. The evaluation result is also shown in Figure 10. In this case, there is no obvious difference in the pupilgram. However, the comparison of the controllability of the OPE change shown in Figure 11 tells us that a value of DPF larger than $10^4$ may be required for the freeform illumination.

## 3.3 Pupilgrams generated by intelligent illuminator unit (IIU)

In the case of the intelligent illuminator, various kinds of pupilgrams can be generated with a single optical element in the illuminator. In addition, the intelligent illuminator has a higher pupilgram modulation freedom than a sPURE-based illuminator. The degree of modulation freedom and pupilgram generation accuracy level are correlated to the degree of pupilgram freedom. Of course, the higher degree of pupilgram freedom corresponds to a higher degree of pupilgram modulation freedom and better accuracy when generating

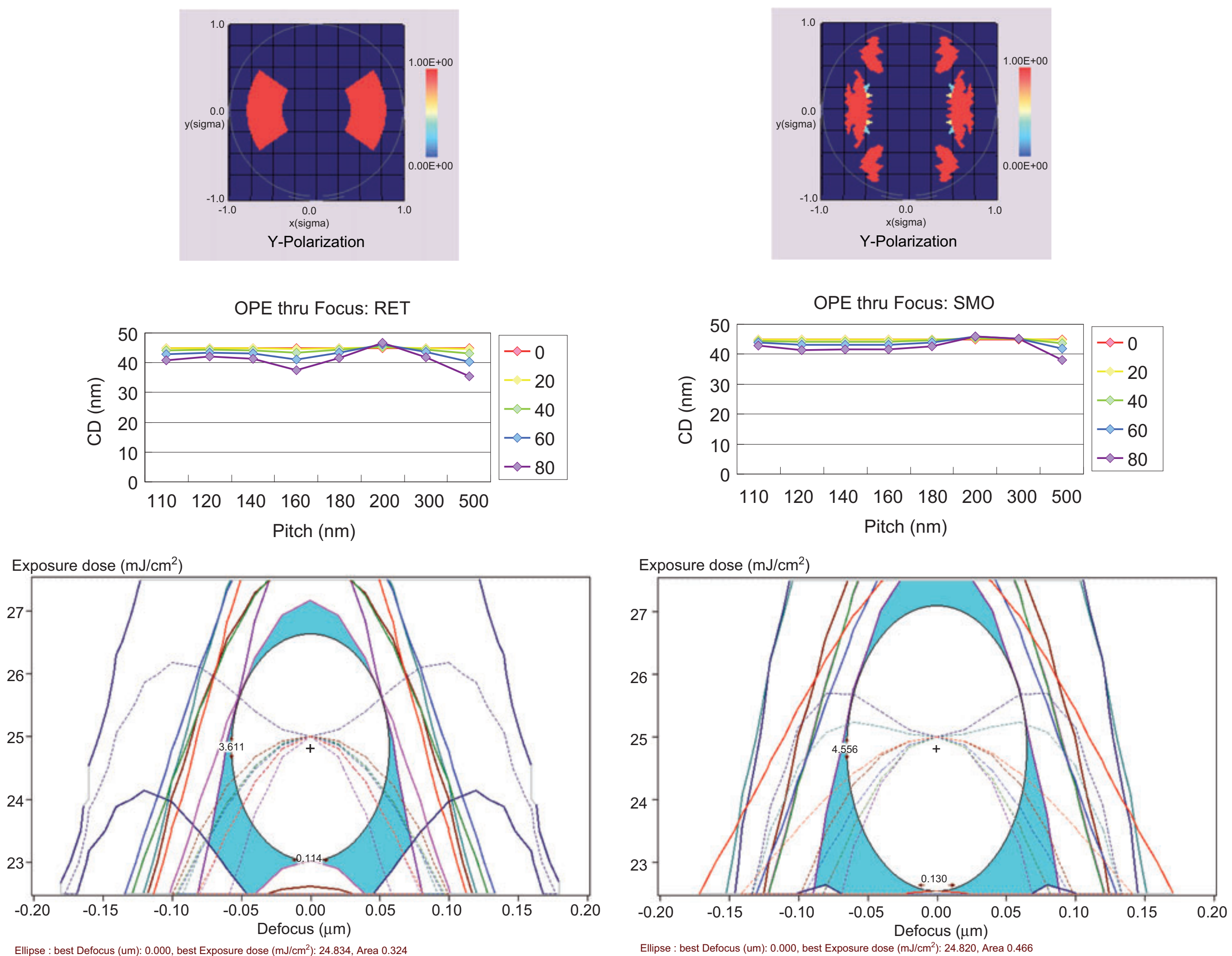


**Figure 7** Imaging performance comparison between conventional RET (left) and SMO (right).

 © 2012 THOSS Media & DE GRUYTER

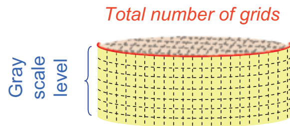


**Figure 8** The degrees of freedom in the pupilgram depends on the number of grid elements and the number of grayscale levels.

the pupilgram. The high degree of pupilgram freedom can be used to realize the freeform pupilgrams accurately and with complex pupilgram modulations to obtain the expected imaging performance characteristics – such as OPE.

Figure 12 shows various kinds of pupilgrams generated by the intelligent illuminator. The upper row shows parametric pupilgrams, which can be defined by the parametric values input into the intelligent illuminator. Parametrically defined illumination intensity distributions, such as the x/y pole intensity balance and the open angle of the fan-shaped pupilgrams, can be modified and demonstrated. The lower row shows the freeform pupilgrams' input by the intelligent illuminator.

## 3.4 Source (and mask) optimization considering pupilgram constraints

Though the intelligent illuminator can generate various kinds of pupilgrams, there are some restrictions. For example, pupil blur size and pupil fill ratio are the main constraints, and these sometimes affect the imaging performance through process margin (process window). However, by taking into account the constraints in the source (and mask) optimization process, the impact of the constraints can be minimized.

## 3.5 Pupilgram predictor

In both the sPURE-based illuminator and the intelligent illuminator, the expected pupilgrams on the scanner are predicted by the pupilgram predictor [3], which gives the point spread function in the pupil as a function of the pupil coordinates and illumination adjusting parameters such as the optical zoom parameters in the illumination system. The optical parameters for the illumination systems are optimized to make the predicted pupilgram as close as possible to the target pupilgram. Furthermore, the illuminator predictor can be used to obtain more robust SMO solutions by using predictor results in the SMO process. In other words, by taking into account the illuminator constraints, the SMO solutions become more robust against the actual illuminator constraints.

The concept of the pupilgram predictor is summarized by Eq. (2) and is further illustrated in Figure 13,

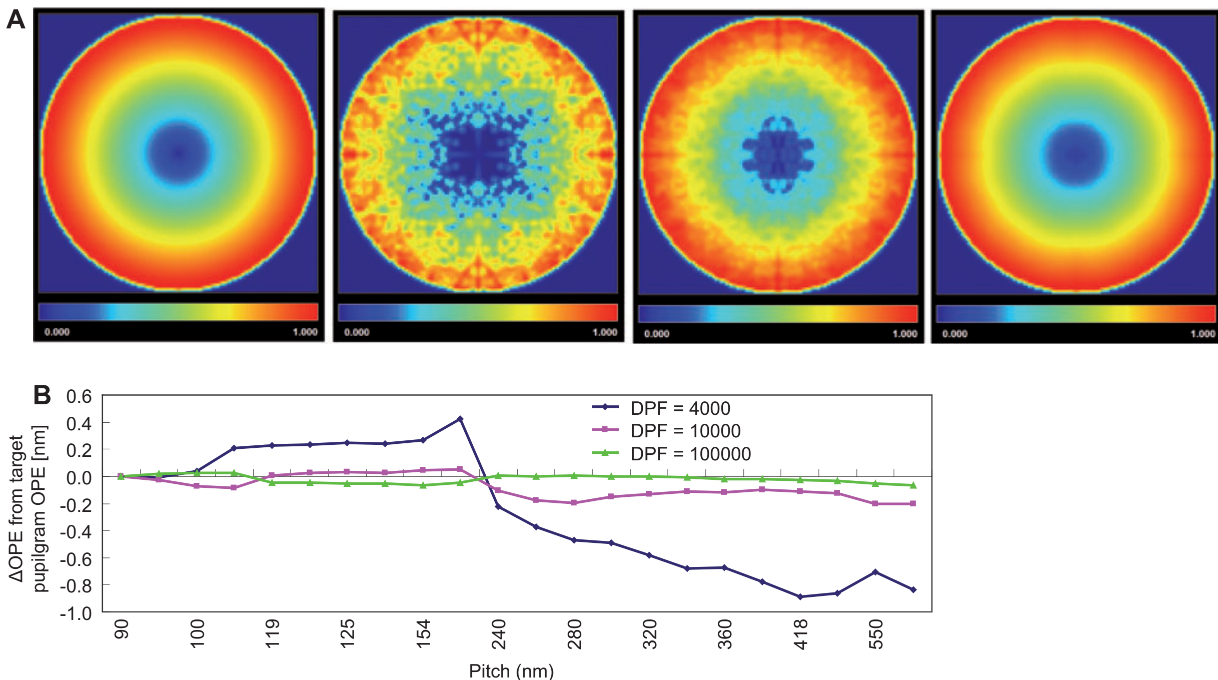


**Figure 9** (A) Generated pupil grams. The far left image is of the target cone-shaped pupilgram, and from left to right shows the pupilgrams with increasing DPF. (B) Comparison of the generated pupilgrams in the OPE change.

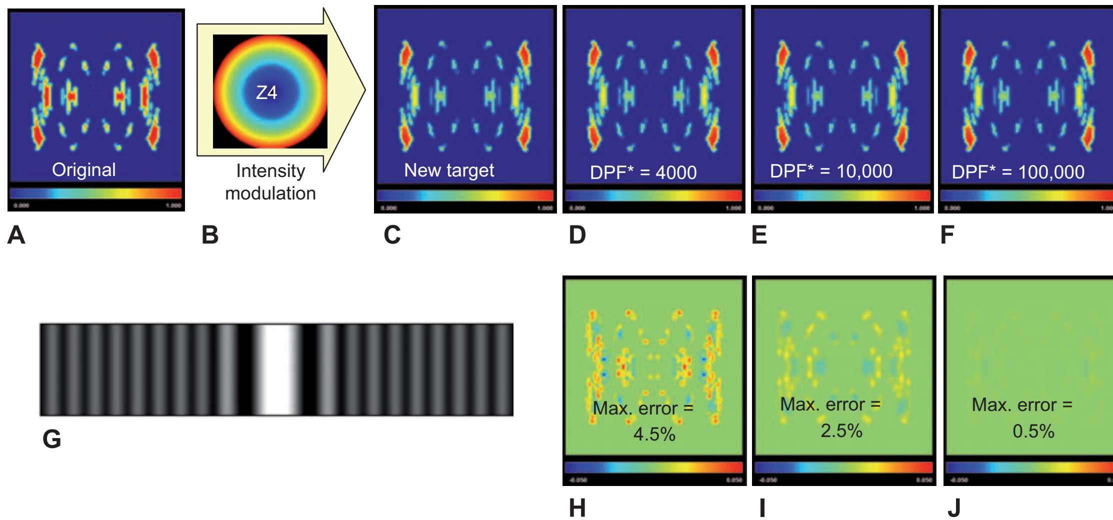


**Figure 10** Example of the SMO using 1D NAND pattern, showing (A) the original illumination, (B) the intensity modulation, (C) the new illumination pattern target, (D–F) representations of the new target source using the increasing DPF, (G) the typical 1D NAND pattern, (H–J) the illumination pattern error for (D–F).

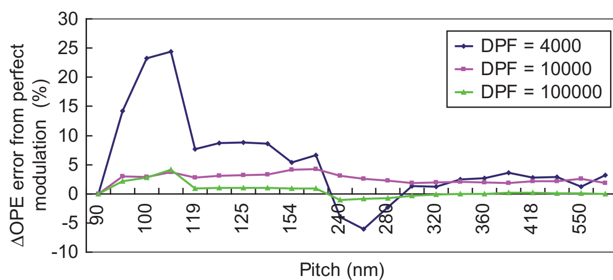


**Figure 11** Change in the OPE from perfect illumination for increasing DPF.

where the predicted pupil $A_{reticle}$, described as a function of the pupil coordinate r, is written in terms of an overlap integral between the far-field sPURE distribution $A_{sPURE}$, expressed in the far-field coordinate ρ, and the illuminator point spread function, psf, which depends on both sets of coordinates as well as the illuminator settings. The illuminator settings can refer to different things for the different illumination systems. For example, it could refer to the pupil magnification or to some annular ratio adjustment.

$$A_{reticle}\left(\vec{r}_{m,n}\right) \approx \sum_{i} \sum_{j} A_{sPURE}\left(\vec{\rho}_{i,j}\right)\ \ psf\left(\vec{r}_{m,n},\vec{\rho}_{i,j};\ settings\right). \quad (2)$$

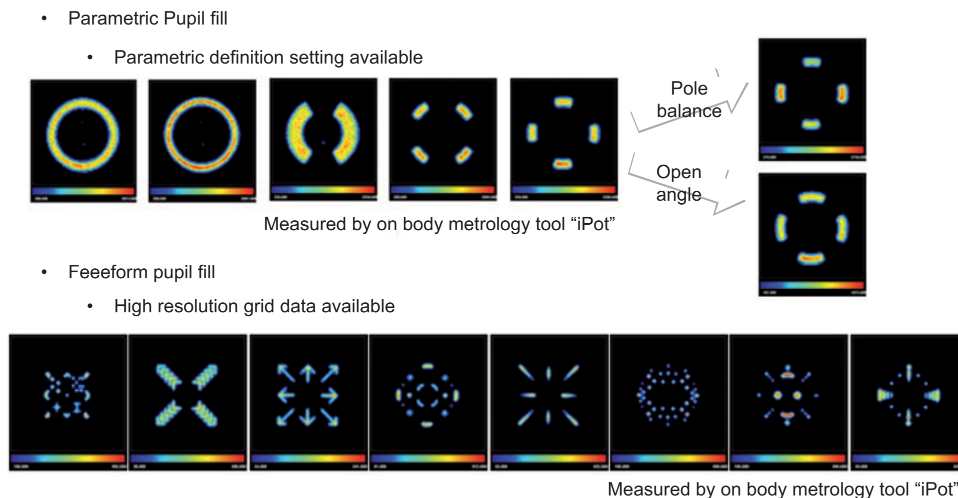


**Figure 12** Various pupilgrams generated by the intelligent illuminator. The upper part illustrates the more conventional parametric pupilgrams. The lower part illustrates the freeform pupilgrams.

 © 2012 THOSS Media & DE GRUYTER

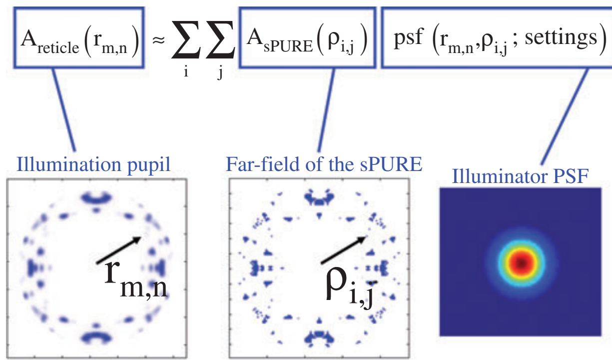


**Figure 13** The prediction of the illumination pupil by overlap integral. The illumination pupil $A_{reticle}$ at each position (m,n) is the result of a summation over all positions (i,j) in the sPURE multiplied by the psf, which depends on the locations of the $r_{m,n}$ and $\rho_{i,j}$, as well as the illuminator settings.

Because the shape of the PSF changes dramatically across the pupil and through the illuminator settings, it is generally shift variant. For this reason, many of the mathematical tools normally used to describe the linear shift invariant systems are not available. So one key in evaluating Eq. (1) quickly is to find a PSF description that is not only accurate but also computationally inexpensive to evaluate.

The pupil predictor must also predict how changes of the illuminator settings affect the illumination pupil and the resulting images at the wafer, enabling OPE matching. The change in the OPE with the annular ratio was computed for the illumination pupils described by the ideal top-hat pupil prescription as well as the predicted pupil and the measured illumination pupil. The results are shown in Figure 14, where the difference in the change of the OPE for the measured pupil is much more accurately represented by the pupil predictor than the top-hat pupilgram. Similarly, the change in the OPE was calculated for a freeform illumination pupil when the pupil magnification was increased by 2.3% and then reduced by 2.3%.

## 4 Pupilgram modulation optimization for OPE matching

In this section, we introduce an OPE matching method that can use the higher degree of pupilgram modulations by the intelligent illuminator unit. We are going to propose a pupilgram modulation model for the OPE matching. Though the model was originally proposed for the pupilgram error analysis [4], it can be used for the freeform pupilgram adjustment for this purpose. In the model, the pupilgram modulation can be expressed by linear combinations of Zernike intensity modulation functions and Zernike distortion modulation functions. These functions are orthogonal and can be expressed by the combination of Zernike polynomials [2]. We also proposed a Zernike linear combination method to predict the OPE response to changes in the pupilgram.

We perform imaging simulations to determine the linearity of the OPE sensitivity and accuracy of the linear

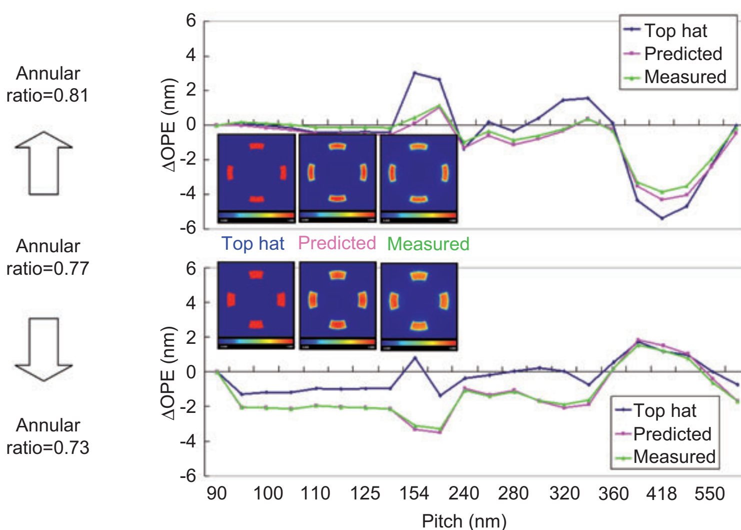


**Figure 14** The change in the OPE when the annular ratio of a c-quad pattern is adjusted from a nominal value of 0.77 to 0.81 (top) and 0.73 (bottom), and for three different illumination pupil descriptions; the ideal top hat (blue), the pupil predictor (pink), and the measured pupil (green).

combination prediction for the OPE. The results show that the Zernike intensity modulation is suitable for the OPE matching in freeform illumination. By using this method, the OPE optimization with a considerable number of variables in the pupilgram can be completed within a reasonable calculation time. In practical cases, OPE matching can be performed after the pupilgram adjustment as the residual pupil distortion may already be small at the time of OPE matching. This is another reason that the intensity modulation may be more effective in compensating the remaining OPE error.

## 4.1 Pupilgram modulation model

We define the modulated pupilgram $I_{modulated}(x,y)$ using the equation below.

$$I_{modulated}(x,y)=T(x,y)[I_{original}(x+D_x(x,y),\ y+D_y(x,y))\otimes PSF]+C \tag{3}$$

where (x,y) is the pupil coordinates,

$I_{original}(x+D_x(x,y),y+D_y(x,y))$ is the original pupilgram intensity distribution,

T(x,y) is the intensity modulation term,

$D_x(x,y)$ is the distortion functions in x,

$D_y(x,y)$ is the distortion functions in y,

PSF is a Gaussian point-spread function in the pupil that generates blur,

C is a constant that expresses the background intensity offset.

In our definition of distortion, the pure shape modulations are expressed without any intensity modulations; it only describes a 'remapping' of the coordinate/pixel positions in the pupil. This equation also defines the hierarchy of the modulation components. The equation is also used for the pupilgram error component analysis, which will be discussed in the last section of this paper.

## 4.2 Zernike intensity modulation functions

The total intensity filtering effect can be expressed by a sum of the component filtering effects $T_i(x,y)$ as

$$T(x,y)=T_1(x,y)\times T_2(x,y)\times\cdots=\prod_i T_i(x,y) \tag{4}$$

where i is a positive integer.

For the intensity modulation, we use the Fringe Zernike functions, which are very familiar in the microlithography industry as a means to express wavefront aberrations. However, the direct use of the Fringe Zernike functions would not be so useful because they take on negative values, which are not realistic for expressing the intensity filtering distribution. In order to make the intensity filtering description physically meaningful, we would need to use a combination of the Fringe Zernike functions as the basis functions, but such combinations are no longer mutually orthogonal.

Therefore, we propose to use the Fringe Zernike functions applied in exponential as,

$$T_m(x,y)\equiv\exp[c_m Z_m(x,y)] \tag{5}$$

where m is a positive integer.

In this case, the negative values of the Zernike functions are physically meaningful and, when zero, give no filtering effect over the entire pupil.

Now, the intensity filtering (modulation) effect can be expressed as a linear combination of the Fringe Zernike functions as the basis functions as shown below.

$$T(x,y)=\exp[c_1Z_1(x,y)]\times\exp[c_2Z_2(x,y)]\times\cdots=\exp\left[\sum_m c_mZ_m(x,y)\right] \tag{6}$$

One example of the effect of the Zernike intensity modulation is shown in Figure 15.

## 4.3 Zernike distortion modulation functions

As for the distortion modulation, we cannot directly use the Fringe Zernike functions as these functions express one-dimensional values, while distortion is two-dimensional as demonstrated by Eq. (7). We, therefore, propose to use the orthogonal distortion functions shown in Table 3. These are expressed by the simple linear combinations of the Fringe Zernike functions and form an orthogonal series. These are the same functions that appear in the Field-Zernike functions [5] for the Z2 and Z3 components. We call these Zernike distortion modulation functions. Some of the pupil distortion functions are graphically illustrated in

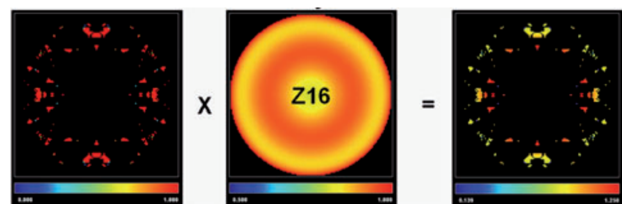


**Figure 15** An example of the application of a single-term (Z16) Zernike modulation function to a freeform illumination pupil.

 © 2012 THOSS Media & DE GRUYTER

| Number | Pupil distortion function |
|---|---|
| Dist. 1 | $(D_{1x}, D_{1y})=(Z1, 0)$ |
| Dist. 2 | $(D_{2x}, D_{2y})=(0, Z1)$ |
| Dist. 3 | $(D_{3x}, D_{3y})=(Z2, Z3)$ |
| Dist. 4 | $(D_{4x}, D_{4y})=(Z2, -Z3)$ |
| Dist. 5 | $(D_{5x}, D_{5y})=(Z3, Z2)$ |
| Dist. 6 | $(D_{6x}, D_{6y})=(Z4, 0)$ |
| Dist. 7 | $(D_{7x}, D_{7y})=(0, Z4)$ |
| Dist. 8 | $(D_{8x}, D_{8y})=(Z5, Z6)$ |
| Dist. 9 | $(D_{9x}, D_{9y})=(Z6, -Z5)$ |
| Dist. 10 | $(D_{10x}, D_{10y})=(Z5, -Z6)$ |
| Dist. 11 | $(D_{11x}, D_{11y})=(Z6, Z5)$ |
| Dist. 12 | $(D_{12x}, D_{12y})=(Z7, Z8)$ |
| Dist. 13 | $(D_{13x}, D_{13y})=(Z7, -Z8)$ |
| Dist. 14 | $(D_{14x}, D_{14y})=(Z8, Z7)$ |
| Dist. 15 | $(D_{15x}, D_{15y})=(Z10, Z11)$ |
| Dist. 16 | $(D_{16x}, D_{16y})=(Z11, -Z10)$ |
| Dist. 17 | $(D_{17x}, D_{17y})=(Z10, -Z11)$ |
| Dist. 18 | $(D_{18x}, D_{18y})=(Z11, Z10)$ |
| Dist. 19 | $(D_{19x}, D_{19y})=(Z9, 0)$ |
| Dist. 20 | $(D_{20x}, D_{20y})=(0, Z9)$ |
| Dist. 21 | $(D_{21x}, D_{21y})=(Z12, Z13)$ |
| Dist. 22 | $(D_{22x}, D_{22y})=(Z13, -Z12)$ |
| Dist. 23 | $(D_{23x}, D_{23y})=(Z12, -Z13)$ |
| Dist. 24 | $(D_{24x}, D_{24y})=(Z13, Z12)$ |
| Dist. 25 | $(D_{25x}, D_{25y})=(Z17, Z18)$ |
| Dist. 26 | $(D_{26x}, D_{26y})=(Z18, -Z17)$ |
| Dist. 27 | $(D_{27x}, D_{27y})=(Z17, -Z18)$ |
| Dist. 28 | $(D_{28x}, D_{28y})=(Z18, Z17)$ |
| Dist. 29 | $(D_{29x}, D_{29y})=(Z14, Z15)$ |
| Dist. 30 | $(D_{30x}, D_{30y})=(Z14, -Z15)$ |
| Dist. 31 | $(D_{31x}, D_{31y})=(Z15, Z14)$ |
| Dist. 32 | $(D_{32x}, D_{32y})=(Z19, Z20)$ |
| Dist. 33 | $(D_{33x}, D_{33y})=(Z20, -Z19)$ |
| Dist. 34 | $(D_{34x}, D_{34y})=(Z19, -Z20)$ |
| Dist. 35 | $(D_{35x}, D_{35y})=(Z20, Z19)$ |
| Dist. 36 | $(D_{36x}, D_{36y})=(Z26, Z27)$ |
| Dist. 37 | $(D_{37x}, D_{37y})=(Z27, -Z26)$ |
| Dist. 38 | $(D_{38x}, D_{38y})=(Z16, 0)$ |
| Dist. 39 | $(D_{39x}, D_{39y})=(0, Z16)$ |
| Dist. 40 | $(D_{40x}, D_{40y})=(Z21, Z22)$ |
| Dist. 41 | $(D_{41x}, D_{41y})=(Z22, -Z21)$ |
| Dist. 42 | $(D_{42x}, D_{42y})=(Z21, -Z22)$ |
| Dist. 43 | $(D_{43x}, D_{43y})=(Z22, Z21)$ |
| Dist. 44 | $(D_{44x}, D_{44y})=(Z28, Z29)$ |
| Dist. 45 | $(D_{45x}, D_{45y})=(Z29, -Z28)$ |
| Dist. 46 | $(D_{46x}, D_{46y})=(Z23, Z24)$ |
| Dist. 47 | $(D_{47x}, D_{47y})=(Z23, -Z24)$ |
| Dist. 48 | $(D_{48x}, D_{48y})=(Z24, Z23)$ |
| Dist. 49 | $(D_{49x}, D_{49y})=(Z30, Z31)$ |
| Dist. 50 | $(D_{50x}, D_{50y})=(Z31, -Z30)$ |
| Dist. 51 | $(D_{51x}, D_{51y})=(Z25, 0)$ |
| Dist. 52 | $(D_{52x}, D_{52y})=(0, Z25)$ |
| Dist. 53 | $(D_{53x}, D_{53y})=(Z32, Z33)$ |
| Dist. 54 | $(D_{54x}, D_{54y})=(Z33, -Z32)$ |
| Dist. 55 | $(D_{55x}, D_{55y})=(Z34, Z35)$ |

**Table 3** Up to the ninth-order pupil distortion functions.

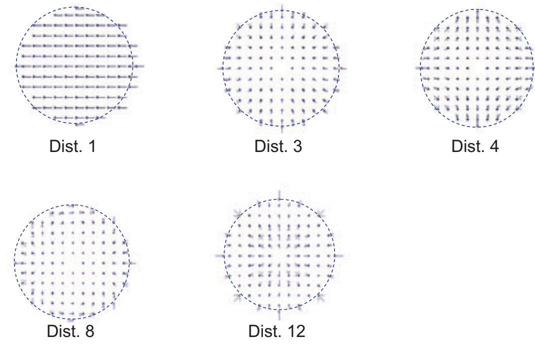


**Figure 16** Several examples of the form of Zernike distortion modulation functions.

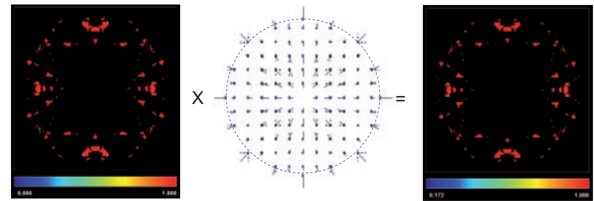


**Figure 17** The application of a Zernike distortion modulation function to a freeform illumination pupil.

Figure 16, and one example of the pupilgram modulation by the Zernike distortion modulation is shown in Figure 17.

$$(D_x(x,y), D_y(x,y)) \equiv \sum d_k (D_{kx}(x,y), D_{ky}(x,y)) \quad (7)$$

## 4.4 OPE matching demonstration by intelligent illuminator

Figure 18 shows the OPE matching results using the pupilgram modulation freedom of the intelligent illuminator with the Zernike distortion modulations and the Zernike

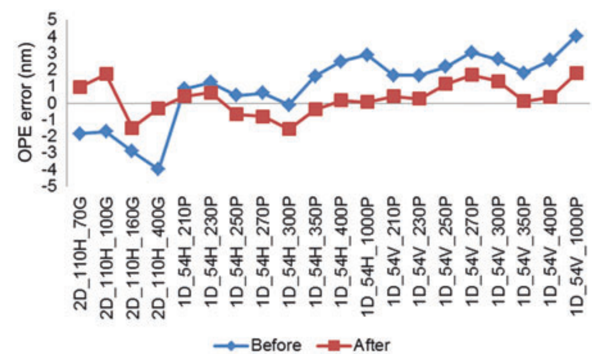


**Figure 18** The OPE matching results using the intelligent illuminator pupilgram modulation freedom.

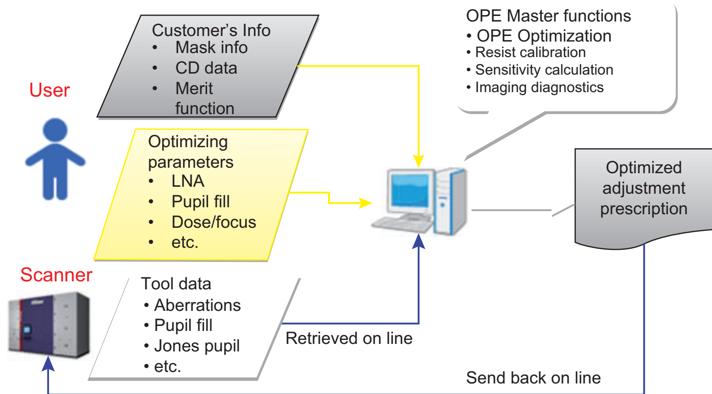


**Figure 19** An overview of the application software 'OPE Master.'

intensity modulations [4]. Though this is a preliminary test of the OPE matching with the intelligent illuminator, we can see the effect of the pupilgram modulations by the intelligent illuminator. The pupilgrams for this experiment use the SMO results assuming typical static random access memory (SRAM) cell pattern.

## 4.5 Application software for OPE matching

In order to use the freedom of the intelligent illuminator effectively, we have developed an application software for the OPE matching using a high degree of pupilgram modulation freedom. We call this application software the OPE Master. Figure 19 indicates an overview of the system. The user can input pattern information, exposed OPE results, and optimization parameters for the OPE matching. The OPE Master automatically retrieves tool-to-match imaging-related tool data for more accurate modeling. The optimization results are also automatically sent back to the scanner.

The OPE Master can optimize the pupilgram modulations generated by the intelligent illuminator such as the Zernike distortion modulation, the Zernike intensity modulation, pupil blur size, and background flare. The pupilgram modulation model is defined by Eq. (3).

The OPE matching validation result is shown in Figure 20. We use the same pupilgrams as used in the preliminary test for the intelligent illuminator. The OPE error can be reduced from 2 nm RMS to 0.7 nm RMS. In the figure, we indicate the pattern size and the pattern pitch in units of nm.

# 5 Summary

We have discussed the effect of the SMO in the expansion of the process window. This is the key technique for achieving even a lower k1 lithography.

The solution of the SMO can be realized in the newly developed illumination system 'intelligent illuminator (IIU)', which has a much higher modulation freedom than a conventional illumination system. The key parameter to define the freedom and accuracy of the pupilgram generation is the 'degree of pupilgram freedom'. The higher

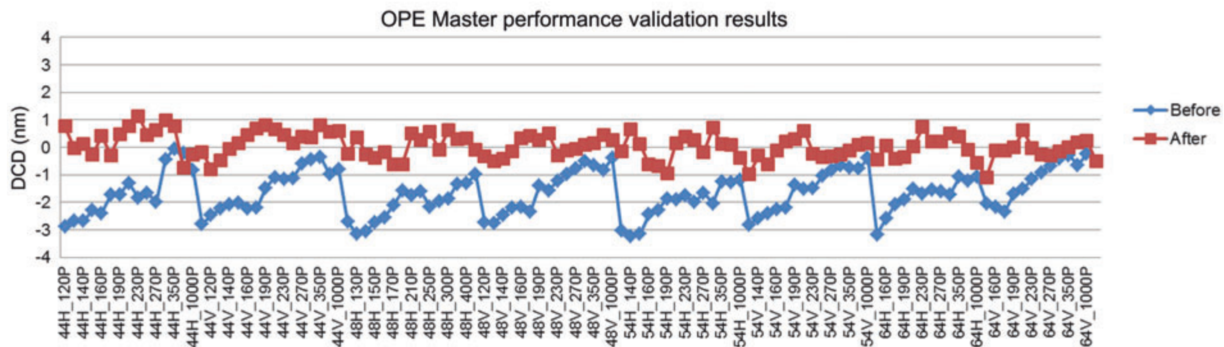


**Figure 20** The OPE matching results using the OPE Master with intelligent illuminator pupilgram modulation freedom.

 © 2012 THOSS Media & DE GRUYTER

DOP indicates a higher degree of pupilgram modulation freedom.

The high modulation freedom IIU can also be used to improve the imaging properties such as the OPE, matching to a reference tool or to a specific design expectation. We demonstrate the setting methods that simultaneously realize high accuracy and high speed. These methods can be used to realize computational lithography in the actual product exposure.

Received July 6, 2012; accepted August 10, 2012

## References

[1] Y. Mizuno and T. Matsuyama, Proc. SPIE 7640, 76401I (2010).
[2] F. Zernike, Physica 1, 689 (1934).
[3] D. G. Smith, N. Kita, N. Kanayamaya, R. Matsui, S. R. Palmer, et al., Proc. SPIE 7973, 747309 (2011).
[4] T. Matsuyama and N. Kita, Proc. SPIE 7640, 764007 (2010).
[5] T. Matsuyama and T. Ujike, Opt. Rev. 11, 199–207 (2004).

Tomoyuki Matsuyama received a BS in applied physics from the University of Electro-Communications (Japan) in 1989. In the same year he joined Nikon Corporation. He has been working in the area of optical design and manufacturing technology development for microlithographic lens. Recently, he is working for development of application software for the imaging system of lithography exposure tool. He is currently a Manager of Imaging Solutions Section, Precision Equipment Company.

Yasushi Mizuno received a BS in mechanical engineering from Tokyo University of Science in 1996 and MS of mechanical engineering from the same university in 1998. In the same year he joined Nikon Corporation in Japan. He is a senior system designer for imaging system of the exposure tool. He is now working for the illumination system development for state-of-the-art ArF immersion scanner.

Daniel G. Smith received his PhD from the Optical Sciences Center and has been working as an optical designer in the field of Microlithography at Nikon Research Corporation of America since 2004.